The Astronomical Journal, 133:845–861, 2007 March

ASYMMETRY AND VARIABILITY IN THE HH 30 CIRCUMSTELLAR DISK[1]

Alan M. Watson[2] and Karl R. Stapelfeldt[3]
Received 2006 May 26; accepted 2006 October 26

ABSTRACT

We consider optical and near-infrared images of the edge-on disk surrounding the young stellar object HH 30 taken with the *Hubble Space Telescope* at 18 epochs from 1994 to 2005. These images allow us to study asymmetry and variability in the disk. The lateral brightness asymmetry in the upper nebula, first seen to strongly vary in 1998, continues to show significant variability throughout the period of our observations. The lateral asymmetry is not uniformly distributed between both sides of the disk; the upper nebula appears brighter on its north-northwest side at 12 epochs, nearly symmetric at four epochs, and brighter on its east-southeast side at only two epochs. This and other evidence indicate that the lateral asymmetry has both static and variable components. The lateral asymmetry shares the overall continuum color of the nebula and is weaker in emission lines than in the continuum. We have searched for periodicity in the sense of the lateral asymmetry. While some possible periods can be excluded, there is no convincing evidence for any specific period. We also consider the lower counternebula. It is as a whole less variable than the upper nebula and shows no significant lateral variability. We discuss several possible mechanisms that might explain these phenomena. Periodic illumination or shadowing models remain viable at periods less than 1 yr, but further observations are required to firmly establish them.

Key words: accretion, accretion disks — circumstellar matter — stars: individual (HH 30) — stars: pre–main-sequence

1. INTRODUCTION

HH 30 is a prototypical young stellar object (YSO) located in the L1551 molecular cloud at a distance of 140 pc. *Hubble Space Telescope* (*HST*) images show that HH 30 is a compact bipolar reflection nebula bisected by a dark lane (see Figs. 1 and 2). Its similarity to the model images of Whitney & Hartman (1992) led immediately to the conclusion that HH 30 is an edge-on, optically thick circumstellar disk. The disk is about 450 AU in diameter, is flared (its vertical thickness increases with radius), and extends perpendicular to the highly collimated bipolar emission-line jets. Using scattered-light models, Burrows et al. (1996), Wood et al. (1998), and Watson & Stapelfeldt (2004) were able to constrain the disk density distribution. These results indicated that the disk is in vertical pressure support with a scale height of roughly 15 AU at 100 AU. Stapelfeldt & Moneti (1999) and Brandner et al. (2000) studied the spectral energy distribution of HH 30 with the *Infrared Space Observatory* and found that direct starlight is completely obscured by the disk for wavelengths less than about 15 μm. Stapelfeldt & Padgett (2001) published millimeter interferometry that showed dense, rotating molecular gas within the optical dust lane. More recently, Pety et al. (2006) published millimeter interferometry that shows both the disk and an asymmetric molecular outflow. Near-infrared imaging by Cotera et al. (2001), in conjunction with scattered-light modeling, found that the opacity of the scattering dust grains decreased less steeply between 1.1 and 2.0 μm than would be expected for interstellar grains. Extensive modeling by Watson & Stapelfeldt (2004) reinforced this result and extended it down to wavelengths of 0.4 μm.

An interesting aspect of the HH 30 system is the prominent time variability in the disk reflection nebulae. Burrows et al. (1996) reported significant changes in the brightness ratio of the upper (north-northeast) and lower (south-southwest) nebulae between 1994 and 1995 and the presence of a weak lateral brightness asymmetry, but did not consider these in any depth. Later, Wood & Whitney (1998) presented a variable-illumination model with nonaxisymmetric stellar accretion hot spots to account for both of these observations and predicted that strong lateral brightness asymmetries should sometimes appear in the HH 30 disk. This prediction was confirmed almost immediately when Stapelfeldt et al. (1999) observed that in 1998 the right (north-northwest) side of the upper reflection nebula brightened dramatically and that the other side faded, relative to 1995. The system had appeared nearly symmetrical about the jet axis in 1995, but in 1998 one side of the disk was 4 times brighter than the other. A weak asymmetry of the opposite sense was seen in the near-infrared images of Cotera et al. (2001).

Using timescale arguments and the absence of changes in brightness gradients adjacent to the dust lane, Stapelfeldt et al. (1999) discounted large-scale motions in the outer disk as the cause of the nebular variability. Instead, they argued that the outer disk acts as a screen on which moving illumination patterns are projected from the inner disk or central star. They considered two possible mechanisms: the bright accretion hot spots of Wood & Whitney (1998) and voids or clumps in the inner disk casting beams or shadows onto the outer disk. Each mechanism can produce an illumination asymmetry that shifts periodically from one side of the disk reflection nebula to the other. Establishing the validity of either variability mechanism would provide an opportunity to study physical processes in an accretion disk system at much smaller spatial scales than can currently be imaged directly.

In addition to the case of HH 30, second-epoch *HST* images have identified six other YSOs with variable reflection nebulosity (Cotera et al. 2007), including three with variable lateral asymmetries. Insights gained in a detailed study of HH 30's variability should thus be applicable to many other objects.

As a step toward understanding the asymmetry in HH 30, we present *Hubble Space Telescope* images of HH 30 from 18 epochs between 1994 and 2005. These images contain a wealth of

[1] Based on observations with the NASA/ESA *Hubble Space Telescope*, obtained at the Space Telescope Science Institute, which is operated by the Association of Universities for Research in Astronomy, Inc., for NASA.

[2] Centro de Radioastronomía y Astrofísica, Universidad Nacional Autónoma de México, Morelia, Michoacán, México.

[3] Jet Propulsion Laboratory, California Institute of Technology, Pasadena, CA, USA.

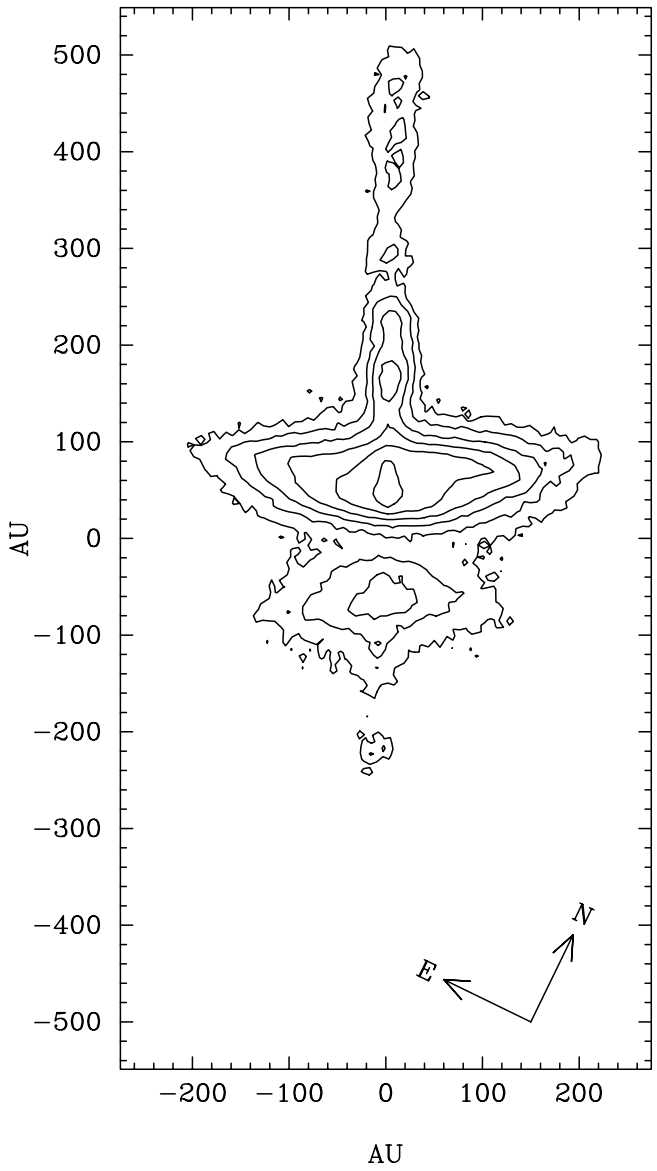

FIG. 1.—*HST* image of HH 30 in the *R* band from 1998 December 27. Contours are spaced by 0.75 from 20.0 mag arcsec^{-2}. The image clearly shows the reflection nebulae associated with the disk and the jet. This is the first image taken at PC resolution through a filter that is sensitive to jet emission.

new information on the HH 30 disk and jet and allow us to study both the variable asymmetry in the disk and the proper motions of the jet knots over an 11 yr baseline. Structure and proper motions in the HH 30 jets will be discussed in a future paper; here we concentrate on variability in the disk reflection nebulae, with the goal of better understanding the nature and mechanisms for the variable asymmetry.

In § 2 we present details of the observations and data analysis. Section 3 describes our photometry. In § 4 we analyze the images and photometry, concentrating on correlations between color and brightness, on the color of the asymmetry, on the vertical profile of the asymmetry, and on possible periods. In § 5 we discuss the implications of our measurements for the properties of the disk and its source of illumination. In § 6 we summarize our results and consider future work.

2. OBSERVATIONS

We consider *HST* observations of HH 30 from 18 epochs over almost 11 yr. Table 1 gives a summary of all the observations. Six epochs have been reported previously (Burrows et al. 1996; Ray et al. 1996; Stapelfeldt et al. 1999; Cotera et al. 2001, 2007). The other epochs are new observations from GO programs 6754, 8289, 8771, 9236, 9863, and 10178, reported here for the first time.

Most of the images were taken with the PC1, WF2, or WF3 cameras of WFPC2 in various combinations of F439W, F555W, F675W, and F814W, the WFPC2 *BVRI* filter analogs. However, there are also two epochs of ACS WFC images in the *R* filter analogs F625W and F606W and two epochs of NICMOS NIC2 images taken in various broadband near-infrared filters. The images from 2005 January were taken through polarizing filters. An intensity image for these epochs was constructed by averaging images taken through polarizers at 0°, 60°, and 120°. Narrowband images were taken with WFPC2 at five epochs, mainly in F656N (Hα) and F673N ([S II]) filters, and with ACS at one epoch in the F658N (Hα+[N II]) filter. The pixel scales of the PC1, WF2/WF3, NIC2, and WFC cameras are approximately 0.046″, 0.097″, 0.076″, and 0.050″. Details of the cameras and filters used at each epoch are given in Table 1.

The WFPC2 images were processed according the prescription of Holtzman et al. (1995b). The ACS images were processed by the *HST* pipeline. In both cases, cosmic rays were eliminated using both a positive-outlier rejection algorithm and by editing the images interactively. A charge trap in the 1994 WFPC2 images resulted in a bad column passing through the upper right portion of the disk; this column was interpolated. The ACS images were corrected for geometric distortion using cubic-convolution interpolation. The NICMOS images were processed with the CALNICA software.

The images were placed on a Vega magnitude scale using zero points from Holtzman et al. (1995a) for WFPC2, Dickinson (1999) for NICMOS, and SYNPHOT for ACS. The background value was estimated for each image by the turning point of a parabola fitted to the peak of the pixel-value histogram.

The images were rotated to have position angle 32° (north-northeast) parallel to the upward vertical. This aligned the disk plane with the horizontal axis and the jets with the vertical axis. The pointing information supplied with the images has errors of roughly 1″ (Burrows 1995), which is large compared to the size of the nebula. Therefore, we aligned all the images by eye, attempting to match the dark lane and the jets. We estimate that worst-case errors in the alignment are about 0.05″.

Images from all 18 epochs are shown in Figure 2. Each column represents an individual epoch of observation, with later epochs to the right. Each row represents a specific wavelength, with longer wavelengths above.

3. PHOTOMETRY

We measured fluxes in five different apertures: a 4″ × 4″ aperture centered on the dark lane and enclosing the entire reflection nebula and four 1.0″ × 1.5″ subapertures displaced 0.15″ above or below and 0.35″ left or right of the center of the dark lane. Thus, the left and right subapertures were separated by 0.7″ to avoid contamination from direct jet emission, and the upper and lower subapertures are separated by 0.3″ to avoid the dark lane. These subapertures are shown in Figure 2. We did not apply aperture corrections, as HH 30 is a resolved source and we are using nonstandard apertures.

From these fluxes we defined seven quantities:

1. The total magnitude $m_{\rm total}$ of the nebula, corresponding to the flux in the 4″ × 4″ aperture.
2. The magnitude of the upper nebula m_u, corresponding to the sum of the fluxes in the two upper subapertures.

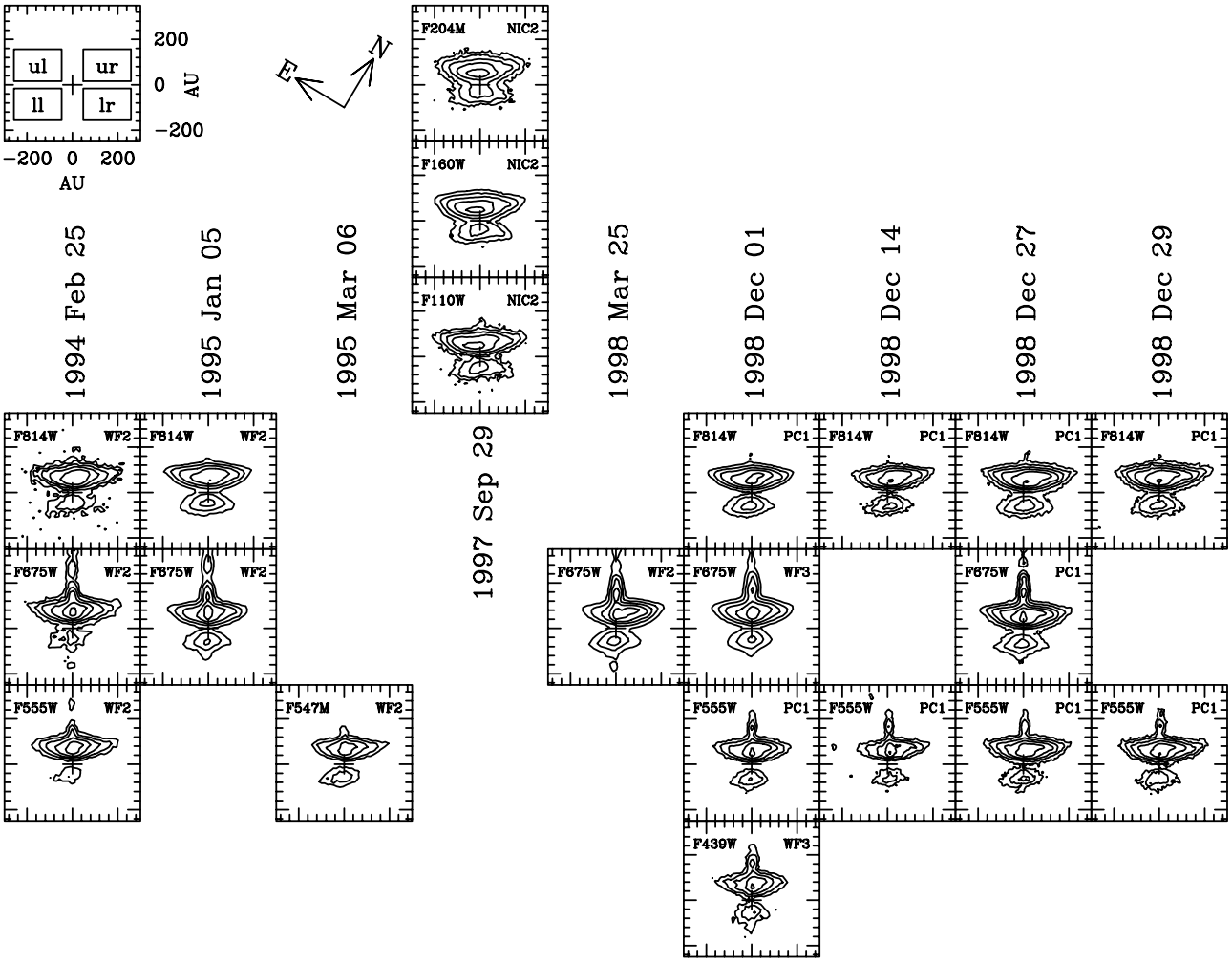

FIG. 2.—*HST* images of HH 30 spanning 18 epochs from 1994 March to 2005 January. Each image in a given column is from the same epoch. Each image in a given row is in the same filter, except that F547M and F555W, and F606W, F625W, and F675W share the same rows. Each image is labeled with the filter and camera used. PC1 images have been smoothed with a 2×2 boxcar filter to suppress noise. The images have been aligned by eye. The cross marks the center of the dust lane, although models suggest that the star is located closer to the brighter nebula. Contours are spaced every 0.75 mag from 22.0 (F439W), 21.0 (F547M or F555W), 20.0 (F606W, F675W, or F625W), 19.5 (F814W), 19.0 (F110W), 17.5 (F160W), or 17.0 (F204M) mag arcsec^{-2}. The top left panel shows the subapertures used to quantify the asymmetry in the nebulae.

3. The magnitude of the lower nebula m_l, corresponding to the sum of the fluxes in the two lower subapertures.

4. The four magnitudes m_{ur}, m_{ul}, m_{lr}, and m_{ll}, corresponding to the fluxes in the upper right, upper left, lower right, and lower left subapertures, respectively.

Thus, the difference $m_u - m_l$ quantifies the contrast between the upper and lower nebulae, and the differences $m_{ul} - m_{ur}$ and $m_{ll} - m_{lr}$ quantify the amplitude of left-right lateral asymmetry in the upper and lower nebulae. These magnitudes and magnitude differences are given in Table 1 and are shown in Figure 3.

One may question whether excluding the region close to the jet might lead to errors in estimating the contrast between the upper and lower nebulae. To investigate this, we performed photometry on the F814W images using apertures that did not exclude this region (i.e., we used a pair of $1.0'' \times 3.7''$ apertures displaced $0.15''$ above or below the dark lane). We selected the F814W images as they are only minimally contaminated by jet emission. The mean difference between the two sets of measurements of the contrast is -0.04 mag (in the sense that the four smaller apertures measure a slightly stronger contrast than the two larger apertures), the rms difference is 0.08 mag, and the largest difference is +0.2 mag (in the sense that the two larger apertures measure a stronger contrast) for the 1994 February 25 epoch. On the basis of these results, we are confident that excluding the jet-axis region does not significantly affect the measurement of the contrast between the upper and lower nebula.

HH 30 is relatively faint, so the uncertainty in the total magnitude is dominated by the uncertainty in the sky level. However, the uncertainties in the magnitudes derived from the subapertures are dominated by uncertainties in the centering. From deliberately miscentered and poorly subtracted images, we estimate worst-case errors of about 0.02 in $m_{\rm total}$, about 0.05 mag for $m_u - m_l$, and 0.2 mag in $m_{ul} - m_{ur}$ and $m_{ll} - m_{lr}$.

4. RESULTS

4.1. *Total Light*

Table 1 and Figure 3 show that the total magnitude of HH 30 varies considerably, with peak-to-peak excursions of 1.2 mag in

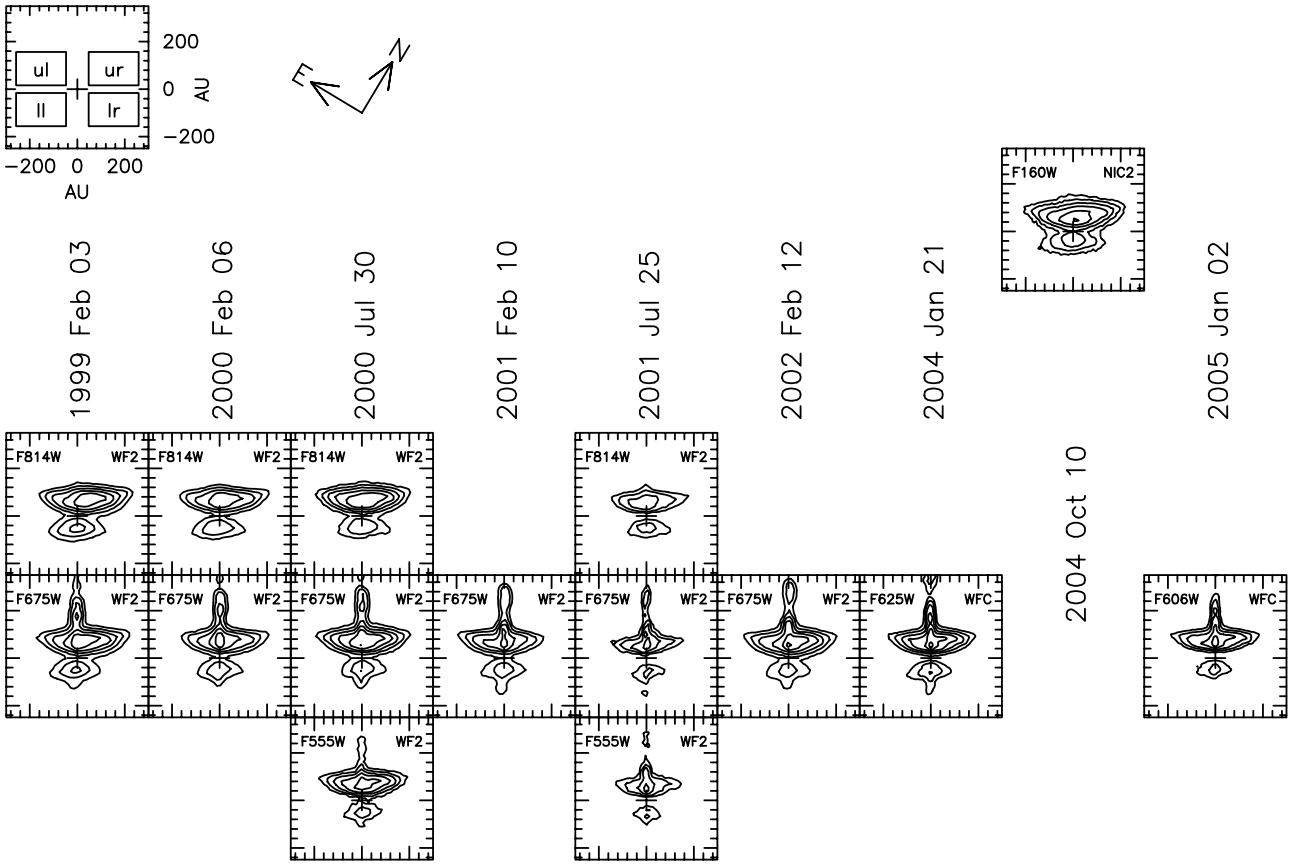

FIG. 2—*Continued*

F555W, 1.3 mag in F675W, and 1.4 mag in F814W. These amplitudes are typical for YSOs.

The WFPC2 F675W filter, the ACS F606W filter, and the ACS F625W filter include strong emission lines such as Hα, [S II], and [O I]. The WFPC2 F555W filter includes much weaker emission lines, and the F814W filter includes almost no emission lines. The F555W − F814W color is thus a good measure of the nebular continuum color. We have images in both F555W and F814W for seven epochs and images in both F675W and F814W for eight epochs.

Figure 4 shows color-magnitude diagrams for the total magnitude (derived from $m_{\rm total}$). The total F555W − F814W color is roughly constant at 1.82 ± 0.13 despite variations of 1.4 mag in F814W.

4.2. *Upper-Lower Contrast*

Table 1 and Figure 5 show that the magnitudes of the upper and lower nebulae, m_u and m_l, also vary considerably. The upper nebula shows greater variability than the lower nebula, with peak-to-peak excursions in m_u of 1.6 mag in F555W, 1.6 mag in F675W, and 1.7 mag in F814W but peak-to-peak excursions in m_l of 0.7 mag in F555W, 0.7 mag in F675W, and 0.7 mag in F814W. The upper nebula is slightly more variable than the total light of HH 30.

Figures 6 and 7 show color-magnitude diagrams for the upper nebula (derived from m_u) and lower nebula (derived from m_l). The F555W − F814W colors are again roughly constant at 1.99 ± 0.09 for the upper nebula and 2.01 ± 0.09 for the lower nebula. Thus, the upper and lower nebula have similar mean colors.

The quantity $m_l - m_u$ measures the contrast between the upper and lower nebulae. The contrast varies with time between 0.80 and 2.12 mag. Figure 8 shows color-magnitude diagrams for the contrast between the upper and lower nebula $m_u - m_l$. The contrast in F555W − F814W colors is 0.06, which is very close to zero, and the spread is entirely attributable to measurement errors. Thus, the contrast appears relatively constant with wavelength at any particular epoch. The one exception is from our observations of 1998 December 1, which show contrasts between the upper and lower nebulae of 1.34 mag in F439W but 1.50 to 1.60 mag in F555W, F675W, and F814W. This is especially strange, as the extinction to the lower nebula is presumably larger (since this would explain its faintness), and this might be expected to produce a larger contrast at shorter wavelengths. Unfortunately, this is our only observation in F439W, and so our ability to determine the significance or origin of the difference is limited.

Figure 5 shows the magnitudes of the upper and lower nebulae m_u and m_l against each other and the contrast $m_l - m_u$ against the magnitudes of the upper and lower nebulae. Figure 5*b* indicates a clear trend for the contrast to be larger when the upper nebula is brighter, with a correlation coefficient of −0.90 for F675W and F606W and −0.95 for F814W (with m_u as the independent variable). However, Figure 5*c* shows that the correlation between the brightness of the lower nebula and the contrast is not as strong, with a correlation coefficient of

TABLE 1

OBSERVATIONS AND PHOTOMETRY

Camera	Filter	Exposure (s)	$m_{\rm total}$	m_u	$m_l - m_u$	m_{ur}	$m_{ul} - m_{ur}$	m_{lr}	$m_{ll} - m_{lr}$
				1994 Feb 25					
WF2	F555W	350	18.21	19.36	+2.10	20.05	+0.13	22.48	−0.48
WF2	F675W	120	16.77	18.01	+1.93	18.71	+0.11	20.91	−0.40
WF2	F814W	60	16.26	17.27	+2.01	17.84	+0.42	20.23	−0.35
				1995 Jan 5					
WF2	F675W	800	17.12	18.51	+1.26	19.22	+0.10	20.66	−0.27
WF2	F814W	1200	16.64	17.72	+1.33	18.43	+0.09	19.94	−0.26
				1995 Mar 6					
WF2	F547M	1000	18.69	19.93	+1.11	20.47	+0.48	22.09	−0.53
WF2	F631N	1800	...	...	+1.95	...	+0.23	...	+0.00
WF2	F656N	3600	...	...	+1.61	...	+0.48	...	−0.45
WF2	F673N	2700	...	...	+1.47	...	+0.17	...	−0.48
				1997 Sep 29					
NIC2	F110W	256	15.77	16.75	+1.37	17.70	−0.36	18.84	+0.06
NIC2	F160W	256	14.39	15.42	+1.28	16.43	−0.47	17.52	−0.13
NIC2	F187N	448	13.62	14.72	+1.30	15.64	−0.32	16.75	+0.04
NIC2	F204M	640	13.76	14.85	+1.31	15.71	−0.20	16.83	+0.17
NIC2	F212N	256	13.57	14.70	+1.26	15.60	−0.28	16.73	−0.03
				1998 Mar 25					
WF2	F675W	2200	16.89	18.05	+1.54	18.26	+1.68	20.46	−0.22
				1998 Dec 1					
WF3	F439W	2400	19.53	20.92	+1.34	21.51	+0.37	23.19	−0.34
PC1	F555W	900	18.42	19.60	+1.60	20.12	+0.53	22.04	−0.16
WF3	F675W	4800	16.96	18.29	+1.50	18.93	+0.23	20.72	−0.34
PC1	F814W	1800	16.61	17.67	+1.52	18.34	+0.17	20.19	−0.44
				1998 Dec 14					
PC1	F555W	300	18.77	20.01	+1.29	20.51	+0.60	22.23	−0.33
PC1	F814W	230	16.80	17.89	+1.35	18.37	+0.65	20.12	−0.24
				1998 Dec 27					
PC1	F555W	520	17.95	19.01	+1.86	19.55	+0.48	21.88	−0.46
PC1	F675W	800	16.61	17.78	+1.77	18.42	+0.23	20.57	−0.49
PC1	F814W	460	16.11	17.06	+1.84	17.51	+0.70	19.74	−0.18
				1998 Dec 29					
PC1	F555W	300	17.94	19.03	+1.93	19.62	+0.34	21.89	−0.34
PC1	F814W	230	16.14	17.13	+1.91	17.74	+0.31	20.02	−0.42
				1999 Feb 3					
WF2	F656N	2000	...	...	+1.79	...	+0.66	...	−0.33
WF2	F673N	2000	...	...	+1.58	...	+0.96	...	−0.07
WF2	F675W	2000	16.77	17.89	+1.79	18.21	+1.19	20.58	−0.27
WF2	F814W	2000	16.32	17.19	+1.80	17.44	+1.47	19.81	−0.13
				2000 Feb 6					
WF2	F656N	2000	...	...	+1.52	...	+0.46	...	−0.12
WF2	F673N	2000	...	...	+1.31	...	+0.39	...	+0.00
WF2	F675W	1923	17.11	18.43	+1.46	18.91	+0.65	20.68	−0.07
WF2	F814W	2000	16.82	17.89	+1.31	18.38	+0.59	20.07	−0.23

TABLE 1—*Continued*

Camera	Filter	Exposure (s)	$m_{\rm total}$	m_u	$m_l - m_u$	m_{ur}	$m_{ul} - m_{ur}$	m_{lr}	$m_{ll} - m_{lr}$
				2000 Jul 30					
WF2	F555W	400	18.10	19.11	+2.08	19.65	+0.48	21.90	+0.09
WF2	F675W	700	16.68	17.79	+2.09	18.33	+0.48	20.59	+0.08
WF2	F814W	400	16.18	17.10	+2.12	17.67	+0.39	19.94	+0.05
				2001 Feb 10					
WF2	F656N	2012	...	...	+1.53	...	−0.05	...	−0.16
WF2	F673N	2120	...	...	+1.23	...	−0.38	...	−0.11
WF2	F675W	2180	17.18	18.48	+1.45	19.52	−0.51	20.75	−0.13
				2001 Jul 25					
WF2	F555W	260	19.13	20.61	+0.92	21.22	+0.30	22.17	+0.25
WF2	F675W	700	17.86	19.40	+0.80	20.07	+0.16	20.92	+0.06
WF2	F814W	400	17.49	18.71	+0.85	19.41	+0.10	20.27	+0.09
				2002 Feb 12					
WF2	F656N	2012	...	...	+1.72	...	+0.39	...	−0.14
WF2	F673N	2120	...	...	+1.55	...	+0.33	...	−0.11
WF2	F675W	2180	16.82	17.96	+1.93	18.42	+0.70	20.68	−0.08
				2004 Jan 21					
WFC	F625W	2456	16.94	18.15	+1.75	18.76	+0.32	20.79	−0.26
WFC	F658N	2328	...	...	+1.81	...	+0.36	...	−0.20
				2004 Oct 7					
NIC2	F160W	49	14.00	14.97	+1.75	15.52	+0.45	17.49	−0.04
				2005 Jan 2					
WFC	F606W	1608	17.37	18.50	+1.73	19.21	+0.09	21.17	−0.34

only −0.27 for F675W and F606W and −0.54 for F814W (with m_l as the independent variable). Thus, variations in the contrast between the upper and lower nebulae are driven mainly by brightening and dimming of the upper nebula.

4.3. *Left-Right Vertical Profile Asymmetry*

Burrows et al. (1996) noted an apparent difference in the vertical profile of the left and right sides of the upper nebula. This difference appears to be persistent and is most clearly seen in Figure 1 and the PC images in Figure 2.

A priori, the difference could be intrinsic to the disk density distribution or be the result of asymmetric illumination. Our F675W images from 2000 February and 2001 February show the asymmetry with similar amplitudes but different senses and allow us to decide between these possibilities. Figure 9 shows the mean profiles of the left and right sides of the nebula and their differences in the 2000 February and the 2001 February F675W images. The profiles were measured in strips from 0.3″ and 1.3″ of the jet axis. In both cases, the peak of the nebular light is clearly shifted upward (away from the disk plane) on the right (north-northwest) side of the disk by about 0.1″ compared to the left (east-southeast) side of the disk. Thus, it appears most likely that the disk is intrinsically asymmetric, possibly because the scale heights are different on the left and right sides or because it is warped upward on the right side.

4.4. *Left-Right Photometric Asymmetry*

The quantities $m_{ul} - m_{ur}$ and $m_{ll} - m_{lr}$ measure the amplitude of any lateral photometric asymmetry in the upper and lower nebulae about the jet axis. Table 1 shows that a variable lateral asymmetry is present in both the upper and lower nebulae.

4.4.1. *Broadband Colors*

Figure 10 shows color-magnitude diagrams for the contrast between the left and right sides of the upper nebula $m_{ul} - m_{ur}$. In this diagram we have plotted magnitudes against independent colors (e.g., F675W against F555W − F814W), since the errors in the individual measurements are large compared to the spread between measurements, and plotting magnitudes against non-independent colors (e.g., F814W against F555W − F814W) can lead to spurious correlations due to correlated errors. In all cases, the mean color of the contrast is not significantly different from zero and the spread is attributable to measurement errors. We can place an upper limit on any systematic color of the contrast of 0.12. Thus, the average color of the asymmetry from F555W to F814W is very close to the color of the whole nebula.

The preceding argument is based on relatively small asymmetries in the range 0.1 to 0.7. However, it also appears to hold for the large asymmetry observed on 1999 February 3, which was observed only in F675W and F814W and so does not appear in Figure 10. At this epoch, the asymmetry was 1.19 in F675W

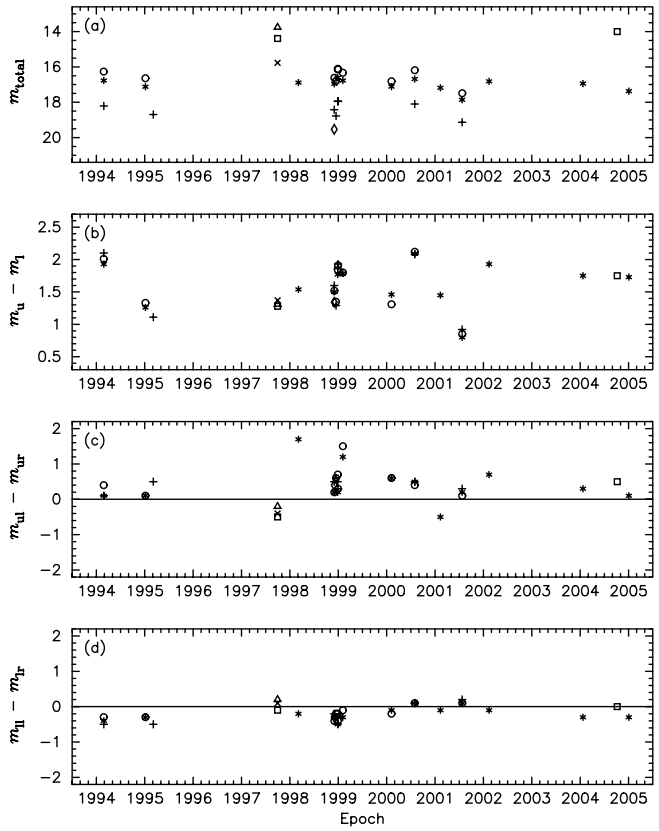

FIG. 3.—Photometry of HH 30. The plots show (*a*) the total magnitude $m_{\rm total}$, (*b*) the difference between the magnitudes of the upper and lower nebula $m_u - m_l$, (*c*) the difference between the left and right sides of the upper nebula $m_{ul} - m_{ur}$, and (*d*) the difference between the left and right sides of the lower nebula $m_{ll} - m_{lr}$. The symbols denote the filter: F439W (*diamonds*), F555W or F547M (*plus signs*), F606W, F675W, or F625W (*asterisks*), F814W (*circles*), F110W (*crosses*), F160W (*squares*), and F204M (*triangles*).

and 1.47 in F814W. Thus, the color in F675W − F814W is 0.28, which is within the worst-case uncertainty of about 0.3.

4.4.2. *Emission Lines*

Images through narrowband filters centered on emission lines are available for seven epochs. The lateral asymmetry is on average weaker in filters containing the strong emission lines of Hα and [S II] than in filters dominated by continuum. This is most dramatically seen in the observations of 1999 February 3 and 2001 February 10. At the first epoch, the asymmetry in F656N is 0.66 whereas the asymmetry in F675W is 1.19, and at the second epoch, the asymmetry in F656N is −0.05 whereas the asymmetry in F675W is −0.51. This behavior clearly indicates that the light making up the asymmetry cannot be dominated by emission lines. The weakness of the asymmetry in emission lines probably arises because the jet is diluting the asymmetry in these filters. The jet stands above the disk and should illuminate the disk equally at all azimuths.

4.4.3. *Distribution*

Unfortunately, HH 30 was not observed with a common filter set over the 18 different epochs of *HST* imaging. Nevertheless, the absence of a strong color dependence in the strength of lateral asymmetry allows us to combine these images to analyze the amplitude distribution and temporal behavior of the lateral asymmetry. Figure 11 shows histograms of the wavelength-averaged value of the amplitudes $m_{ul} - m_{ur}$ and $m_{ll} - m_{lr}$ at each epoch (i.e., the average of these measurements in the broadband and medium-band filters at each epoch). In the upper nebula the distribution of $m_{ul} - m_{ur}$ is shifted to positive values, with a mean of +0.42 mag, a worst-case uncertainty of about 0.05, and a median of +0.45 mag. The upper nebula shows a negative lateral asymmetry ($m_{ul} - m_{ur} < 0$) at only two of the 18 epochs. In the lower nebula, however, the distribution of $m_{ll} - m_{lr}$ is shifted to negative values, with a mean of −0.21 mag, a worst-case uncertainty of about 0.05, and a median of −0.24 mag. The lower nebula shows a positive lateral asymmetry ($m_{ul} - m_{ur} > 0$) at only three of the 18 epochs.

We can investigate the significance of these nonzero means by hypothesizing that the lateral asymmetry in the upper nebula is randomly distributed between the left and right sides. Under this hypothesis, the probability of 2 or fewer of 18 unambiguous observations showing the same sign for the asymmetry is only 0.001. If we assume that the 1998 December observations are not independent (i.e., that the correlation time for the asymmetry is 1 month or longer) and treat them as a single observation, then the probability of 2 or fewer out of 15 observations showing the same upper asymmetry is only 0.007. If we assume that the 1998 December and 1999 February observations are not independent and that the 1995 January and 1995 March observations are not independent (i.e., that the correlation time is 2 months or longer), then the probability of 2 or fewer out of 13 observations showing the same upper asymmetry has a probability of 0.022. These low

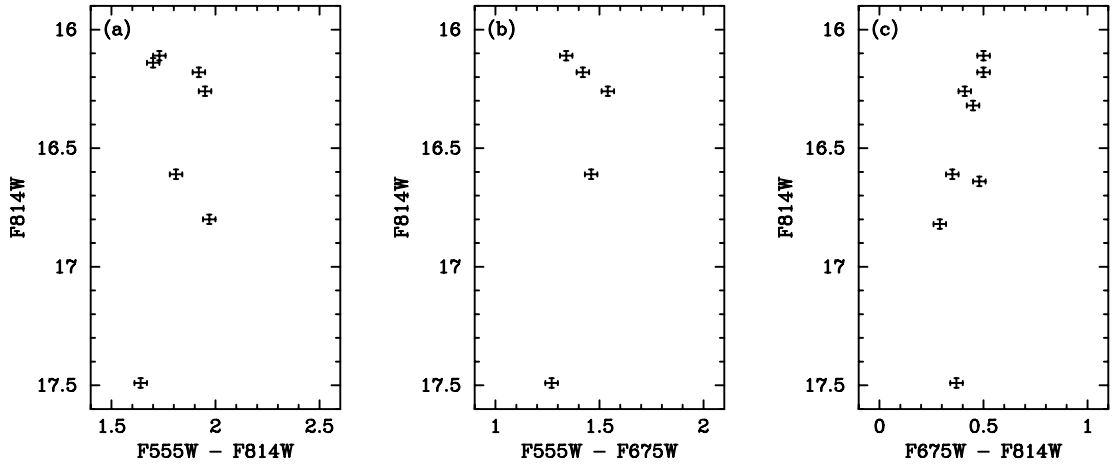

FIG. 4.—Color-magnitude diagrams for the total magnitude of the nebula $m_{\rm total}$.

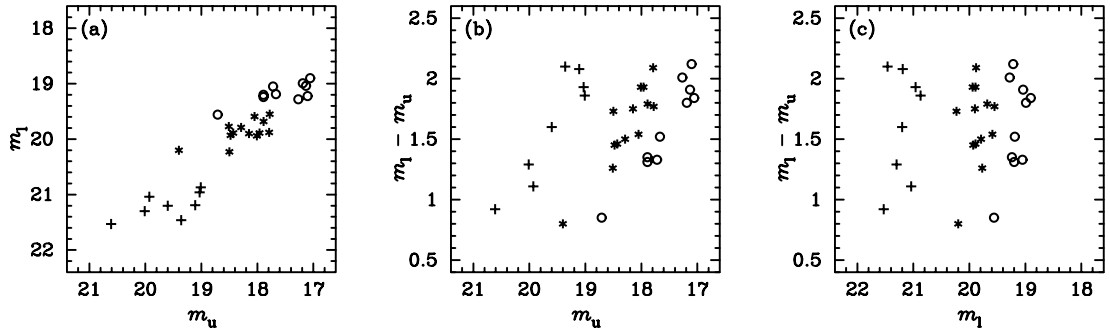

FIG. 5.—Plots of the magnitudes of the upper and lower nebulae, m_u and m_l, and the contrast $m_l - m_u$. The symbols denote the filter: F555W or F547M (*plus signs*), F606W, F625W, or F625W (*asterisks*), and F814W (*circles*).

probabilities strongly suggest that the upper asymmetry is not uniformly distributed between the left and right sides of the upper nebula. Similar conclusions apply to the lower nebula.

Apart from the sign of the mean, the upper and lower distributions appear to differ in their width, with the distribution of the upper asymmetry being considerably broader. The standard deviation of the upper nebula asymmetry is 0.51 mag, and the largest deviation from the mean in the upper nebula is 1.27 mag (at the epoch discussed by Stapelfeldt et al. 1999). In the lower nebula, the standard deviation is only 0.17 mag for the lower nebula and is entirely consistent with measurement errors. Thus, there is no significant variable asymmetry in the lower nebula.

4.4.4. *Possible Periods*

It is possible that the asymmetry is periodic. We would like to search for all periods that are consistent with the data, but in this we face two difficulties: we cannot use a model for the shape of the light curve, as this may depend sensitively on the details of the illumination, and there are uncertainties of ± 0.2 mag in our measurement of the asymmetry. Furthermore, the mechanism might be periodic but lack phase stability (see Herbst et al. 1994 and references therein).

For these reasons, we have adopted a simple model. We assume that the asymmetry is more negative than its mean value of +0.42 for half of one period and more positive for the other half. We average the value of $m_{ul} - m_{ur}$ in the broadband and medium-band filters at each epoch, and we consider the sense of the variable asymmetry to be reliably determined only when it differs by more than 0.2 mag from the mean. Figure 12 shows the wavelength-averaged asymmetry in the upper nebula as a function of time, along with the band at $+0.42 \pm 0.2$. We then search for possible periods and phases that correctly predict the sense of reliable measurements. In searching for periods, we assume that there have been no phase shifts over 11 yr.

We have searched for periods and initial phases between 0.01 and 10,000 days that satisfy the sense of the asymmetry at all epochs. We examined all periods spaced by 10^{-4} in the log and all relative phases spaced by 10^{-4} of a period. Allowed periods and phases (at a Julian day of 0) are marked in black in Figure 13. It can be seen that this plot places very limited constraints on the period; a large range of periods are allowed. The space below about 80 days is densely filled with allowed periods, and then there are allowed bands with periods around 102 days, around 140 days, and around 300 days.

Independent of this analysis, there are two important observations that give insights into short timescales for variability. First, *HST* observed HH 30 on 1998 December 1 during each orbit for over 5 hr, and no major changes were seen in the asymmetry. This suggests that the asymmetry remains constant over timescales of hours, although further observations would be needed to firmly establish this. Second, there appears to be a small decrease in the asymmetry between 1998 December 27 and 29, with the mean asymmetry dropping from 0.47 to 0.33. Figure 14 shows the F555W images from these two epochs along with their difference (after scaling the 1998 December 29 image to have the same m_u as the 1998 December 27 image). The difference image shows that the asymmetry was indeed stronger in the earlier epoch. We investigated alignment errors; the relatively strong jet

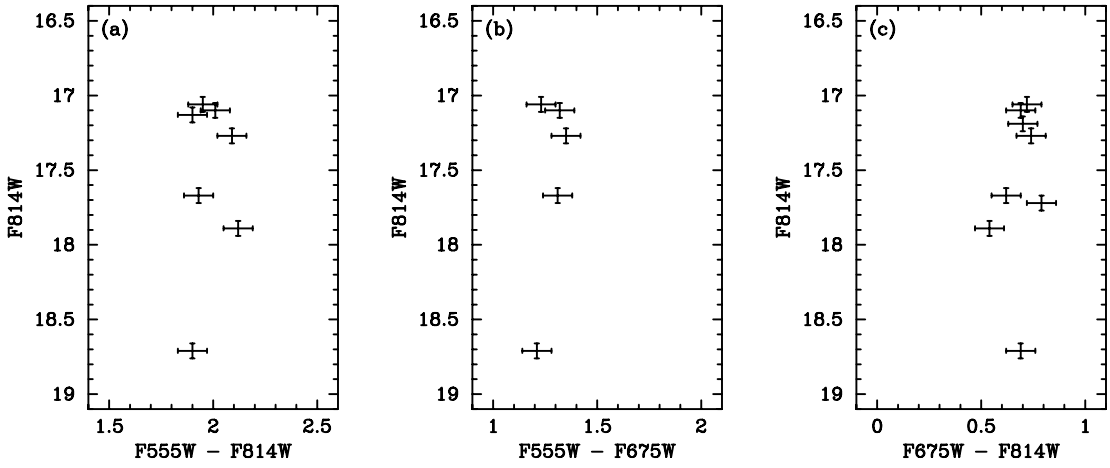

FIG. 6.—Color-magnitude diagrams for the magnitude of the upper nebula m_u.

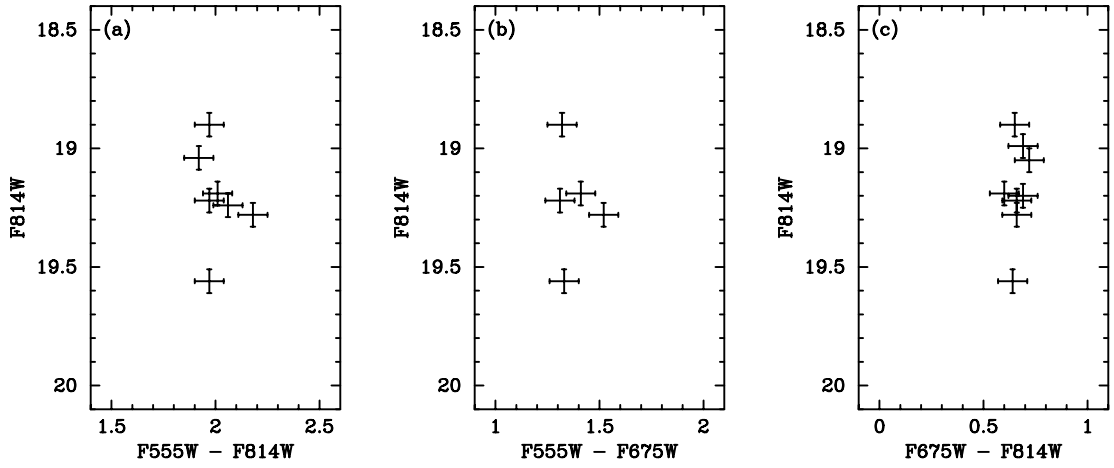

FIG. 7.—Color-magnitude diagrams for the magnitude of the lower nebula m_l.

emission places firm limits on these and allows us to confirm that the decrease is real. Taken together, these observations would tend to favor shorter periods of order 10 days; it seems unlikely that the amplitude would be roughly constant over 5 hr if the period were 1 day or less, and it seems unlikely that a decrease could be observed in just 2 days if the period were 100 days or more. However, the amplitude of the asymmetry may well reflect both the phase (orientation of the beam to the line of sight) and the brightness of the asymmetric source (which might vary stochastically, as is common in YSOs). If this were the case, short-term variations in the amplitude would not necessarily indicate a short period.

4.4.5. *Correlations*

Figures 15*a* and 15*b* show the relation between the amplitude of the asymmetry in the upper nebula and either the total magnitude or the magnitude of the upper nebula. There appears to be a weak trend for the asymmetry to be more positive when the nebula is brighter. However, the linear correlation coefficients r between $m_{ul} - m_{ur}$ and $m_{\rm total}$ (with $m_{\rm total}$ as the independent variable) are only -0.34 for F675W and F606W and -0.34 for F814W, indicating that there is a large degree of scatter. The absence of a clear correlation between the integrated brightness of the nebula and the magnitude of the lateral asymmetry implies that it will be difficult to use integrated photometry of HH 30 to study the asymmetry.

The linear correlation coefficients r between $m_{ul} - m_{ur}$ and m_u (with m_u as the independent variable) are similar, being -0.38 for F675W and F606W and -0.34 for F814W. The nonzero mean of the asymmetry in the upper nebula does not affect the correlation coefficient, as the model for the linear coefficient allows for an arbitrary displacement of the origin. The absence of a clear correlation between the integrated brightness of the nebula and the magnitude of the lateral asymmetry implies that time-series photometry of HH 30's integrated light cannot be used to study the variable asymmetry.

Figure 15*c* shows the relation between the amplitude of the asymmetry in the lower nebula and the magnitude of the lower nebula. The linear correlation coefficient r of $m_{ll} - m_{lr}$ against m_l (with m_l as the independent variable) is only -0.09 for F675W and F606W and -0.14 for F814W, indicating that scatter is dominant. Figure 15*d* shows the relation between the asymmetries in the upper and lower nebulae. The linear correlation coefficient r between $m_{ll} - m_{lr}$ and $m_{ul} - m_{ur}$ (with $m_{ul} - m_{ur}$ as the independent variable) is only 0.08 for F675W and F606W and 0.12 for the F814W observations, indicating that once again scatter is dominant. Since the width the distribution of the lower asymmetry is consistent with the observational errors, these low-correlation coefficients are not surprising.

Figure 15*e* shows the relation between the asymmetry in the upper nebula and the upper-lower contrast. The linear correlation coefficient r between $m_l - m_u$ and $m_{ul} - m_{ur}$ (with $m_{ul} - m_{ur}$ as

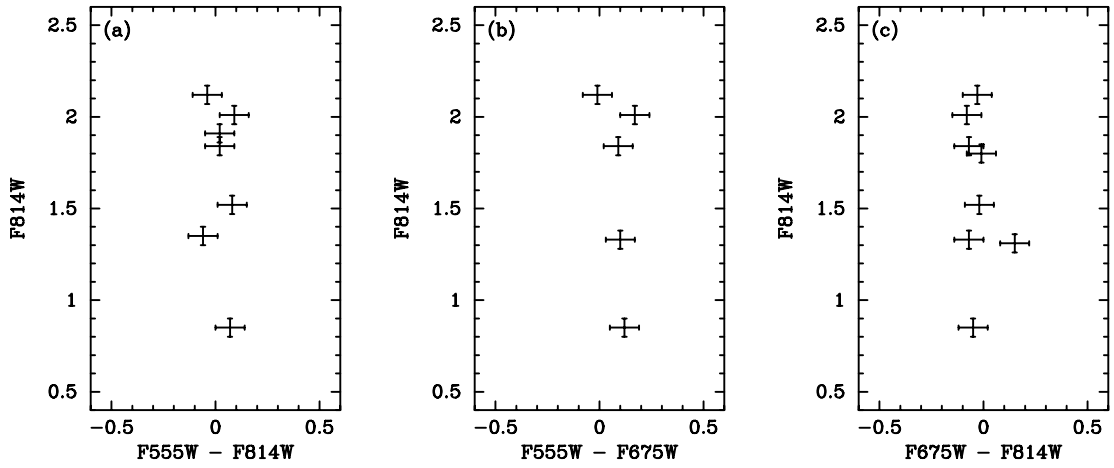

FIG. 8.—Color-magnitude diagrams for the contrast between the upper and lower nebulae $m_u - m_l$.

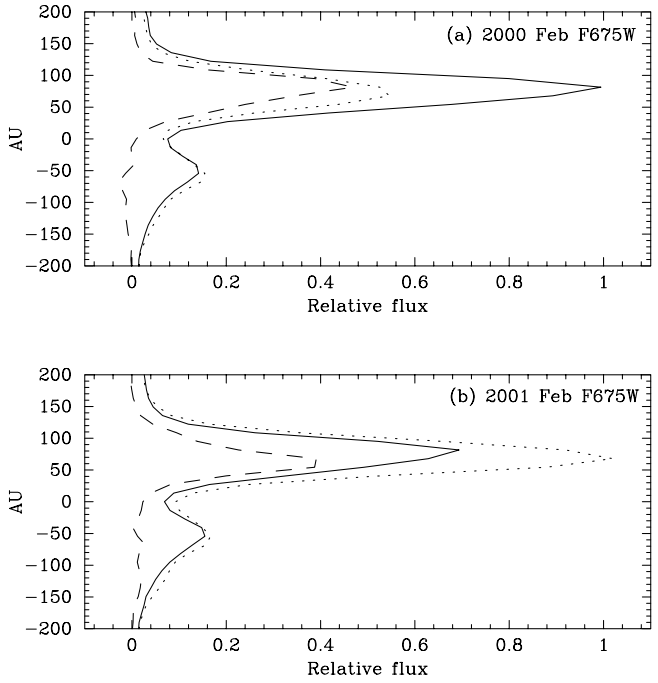

FIG. 9.—Vertical brightness profiles of the right (*solid line*) and left (*dotted line*) sides of the (*a*) 2000 February F675W image (with the right side brighter) and (*b*) 2001 February F675W image (with the left side brighter). The dashed line shows the difference. The flux units are arbitrary.

the independent variable) is only 0.20 for F675W and F606W and 0.32 for the F814W observations, again indicating that scatter is dominant.

4.5. *Summary*

Given the range of behavior seen in HH 30, we consider it useful to summarize our main observational results as follows.

1. The total magnitude of HH 30 in F814W ranges from 16.1 to 17.5, but its color in F555W − F814W is roughly constant at about 1.82.

2. The lower nebula varies by up to 0.7 mag, and the upper nebula varies by up to 1.7 mag. The contrast between the upper and lower nebulae varies from about 0.8 to 2.1 mag in F814W. The variability in the contrast seems to be largely driven by the upper nebula. The contrast does not depend strongly on wavelength between F555W and F814W.

3. The mean amplitudes of the lateral asymmetry in the upper and lower nebulae are not zero, but are about +0.42 in the upper nebula and −0.21 in the lower nebula. That is, the right side of the upper nebula is on average brighter than the left side, and the left side of the lower nebula is on average brighter than the right side.

4. There is a variable lateral asymmetry in the upper nebula. This is not strongly correlated with either the total magnitude, the magnitude of the upper nebula, or the contrast between the upper and lower nebulae. It differs from the global colors of HH 30 by less than 0.2 in F555W − F814W and does not appear to be dominated by emission lines. Its amplitude is large, reaching at least 1.7 mag in total or 1.3 mag above the mean. The variability about the mean is consistent with periods of up to about 300 days, and there is evidence that its amplitude can change by about 0.2 mag in just 2 days.

5. There appears to be no correspondingly large variable lateral asymmetry in the lower nebula.

6. The vertical profiles of the left and right sides of the upper nebula are different, but are unaffected by the lateral photometric asymmetry.

5. DISCUSSION

5.1. *The Nature of the Illuminating Source*

The observed color of HH 30 in F555W − F814W is roughly constant at 1.82 ± 0.13. This color is determined by at least three factors: the intrinsic color of the central source (the stellar photosphere plus veiling continuum), possible chromaticity in the scattering of starlight from the disk, and foreground reddening in the interstellar medium or a diffuse envelope.

White & Hillenbrand (2004) obtained high-resolution spectra of HH 30. Their analysis suggested that the spectral type of the star is K8–M2, and that the veiling component was dominant at 6500 and 8500 Å at the time of their observations, being roughly 5 times as bright as the photosphere. Since the observed colors of HH 30 do not appear to change with its magnitude, either the veiling component must be dominant at all epochs or the veiling component and the photosphere must have very similar $V - I$ colors. Both of these possibilities are consistent with the observations and analysis of White & Hillenbrand (2004).

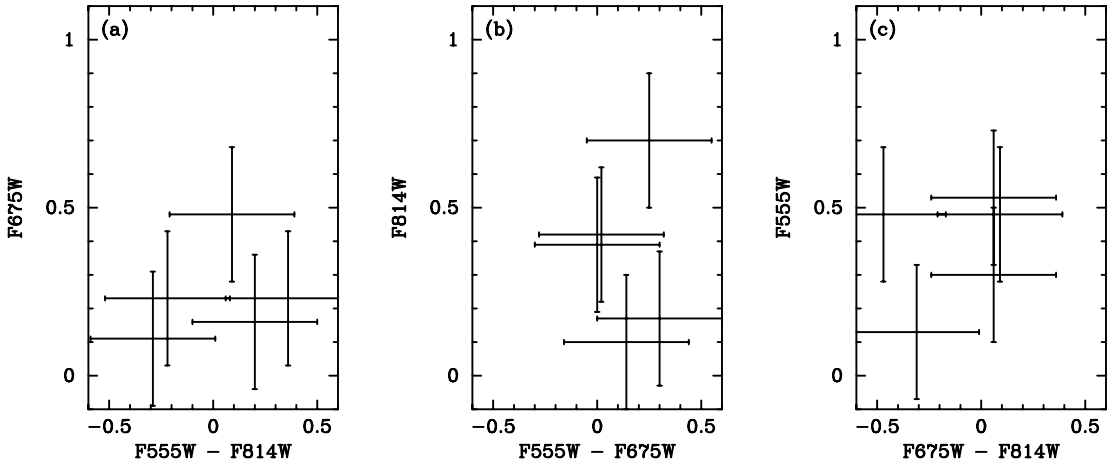

FIG. 10.—Color-magnitude diagrams for the asymmetry in the upper nebula $m_{ul} - m_{ur}$. Note that the data plotted as the ordinate are independent of the data plotted as the abscissa to avoid spurious effects due to correlated errors.

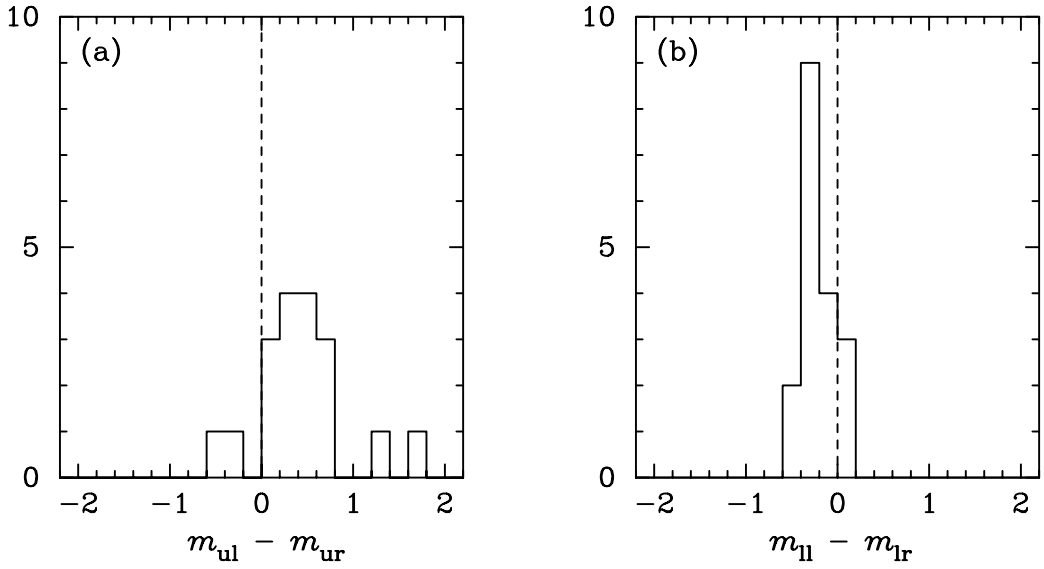

FIG. 11.—Histograms of (*a*) the wavelength-averaged asymmetry in the upper nebula $m_{ul} - m_{ur}$ and (*b*) the wavelength-averaged asymmetry in the lower nebula $m_{ul} - m_{ur}$ in the broadband and medium-band filters at each epoch. Notice that the distributions are not centered on zero.

We can estimate the likely range of the intrinsic color of the illuminating source (i.e., the photosphere and veiling continuum) by taking the likely range of the intrinsic $R - I$ color of the K8–M2 star of +0.7 to +1.1 (Thé et al. 1984) and applying reddening or blueing corresponding to oppositely signed 1 σ variations in the veiling measurements of White & Hillenbrand (2004), which allow the source to be −0.3 mag bluer or +0.4 mag redder than the star alone. The final range of likely intrinsic $R - I$ colors of the illuminating source is +0.4 to +1.6.

The wavelength dependence of scattering by the optically thick disk has been modeled by Watson & Stapelfeldt (2004). Interestingly, the disk colors between 0.44 and 0.81 μm and between 0.81 and 2.04 μm are predicted to be almost zero, with almost all values between +0.1 and −0.1 mag. The absence of a strong wavelength dependence is characteristic of optically thick scattering with an unseen illuminating source; at all wavelengths, scattering takes place near $\tau = 1$, and thus the dust opacity's wavelength dependence is irrelevant. Since the direct light from the illuminating source is not contributing, there is no reddening effect, and there is no enhanced blue scattering as in the optically thin, small-particle case. A caveat is that nonzero colors can still arise from a wavelength-dependent albedo, but this is believed to be only a 10% effect between 0.5 and 1.0 μm (Whitney 1995). Thus, the disk is unlikely to alter the intrinsic $V - R$ color of the illuminating source by any more than 0.1 mag. The likely range of $V - R$ for starlight reflected by the disk is thus +0.3 to +1.7 mag.

Our observations of the F675W − F814W colors of HH 30 are significantly contaminated by jet emission, but our F555W − F814W colors are not significantly contaminated. Therefore, we assume that the observed $V - R$ color of the disk in the absence of jet contamination is half the observed F555W − F814W color. The resulting color of about +0.9 mag lies within the likely range of intrinsic colors of the system, and so is consistent with no foreground reddening or extinction. On the other hand, an intrinsic $R - I$ of +0.3 for the system would require about 0.6 mag of reddening between R and I, which would suggest a foreground extinction in I of about 1.8 mag (Holtzman et al. 1995a).

Strom et al. (1989) gave observed I magnitudes for classical T Tauri stars in Taurus in the range of 7.2–12.7. The F814W magnitude of HH 30 varies between about 16.1 and 17.5, making it roughly 3.4–10.3 mag fainter than comparable, directly visible T Tauri stars. At most 1.8 mag of this is attributable to foreground extinction; the rest must be the result of dilution of light from the source by the disk. The models of Watson & Stapelfeldt (2004) indicate that the integrated brightness of disk scattered light could be 3–8 mag fainter than direct starlight, with a strong peak at 3.5 mag, and so the difference between HH 30 and the sample of Strom et al. is consistent with the dilution of light by the disk.

In summary, the mean values and variability of the integrated colors and magnitudes of HH 30 are consistent with it being a normal, albeit heavily veiled, classical T Tauri star that suffers up to 1.8 mag of foreground extinction in I and heavy dilution by its edge-on disk.

5.2. *Static Lateral Asymmetries*

Observations of the upper nebula of HH 30 provide evidence for two static lateral asymmetries. First, measurements of the

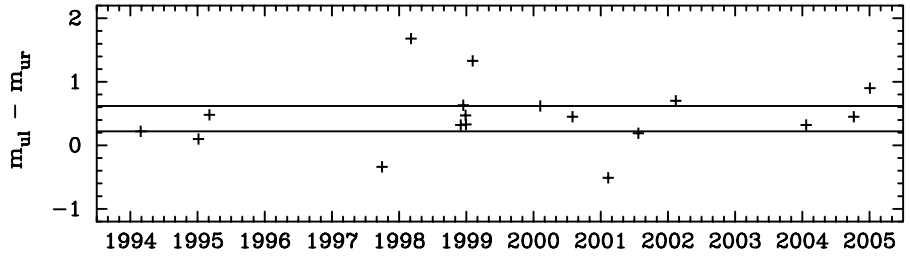

FIG. 12.—The wavelength-averaged asymmetry in the upper nebula $m_{ul} - m_{ur}$ in the broadband and medium-band filters at each epoch. Notice that the distribution is not centered on zero. The lines at +0.21 and +0.61 show the region in which the sense of the asymmetry is uncertain.

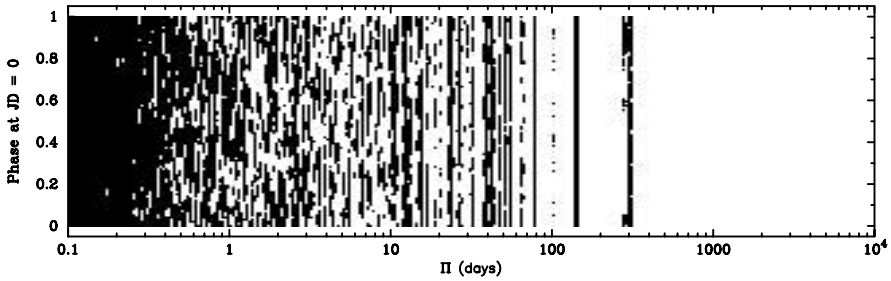

FIG. 13.—Allowed periods and relative phases for the variable lateral asymmetry.

lateral photometric asymmetry over 18 epochs show that it is not evenly distributed about zero. Instead, the mean asymmetry is +0.42. Either light is preferentially illuminating the right (north-northwest) side of the upper nebula or this region of the disk is more efficient in diverting light toward the observer. Second, the right (north-northwest) side of the upper nebula has its photometric center displaced upward by about 0.1″ with respect to the left side of the upper nebula. Occam's razor suggests that these two asymmetries are related. We refer to these as static asymmetries, meaning "static over the timescale of our observations," contrasting them with the variable asymmetry discussed below.

The lower nebula has a mean asymmetry of −0.21 mag and shows a greater out-of-plane extent to its left (east-southeast) side in the images of Burrows et al. (1996). It appears at first sight that the lower nebula might have a point-symmetric counterpart to the static asymmetry in the upper nebula. However, at least when viewed from the position of Earth, this counterpart appears to be not as pronounced as the asymmetry in the upper nebula, which suggests that any point symmetry is not perfect.

A static disk asymmetry might be expected to also be present in thermal emission form the disk. Both Stapelfeldt & Padgett (2001) and Pety et al. (2006) have obtained millimeter interferometry of HH 30, but their results give conflicting pictures of asymmetry in the disk. The integrated ^{13}CO 2–1 map of Stapelfeldt & Padgett shows that the peak line emission from the disk is offset to the right (north-northwest) of the 220 GHz continuum emission. However, the maps of the same transition by Pety et al. are much more symmetric, with only a slight enhancement to the left (east-southeast) side (see their Fig. 8).

The 1979 polarimetry of Cohen & Schmidt (1981) showed that HH 30 is linearly polarized by 3% at a position angle of 93°. The models of Whitney & Hartmann (1992) indicate that a symmetric edge-on disk nebulosity should show a net polarization that is perpendicular to the disk plane, which would be at a position angle of 32° for the case of HH 30. Their model polarization vector maps suggest that the difference in polarization position angle between the 1979 observations and the predicted value could be explained by the upper right nebula being brighter than the upper left nebula, which is exactly the sense of the mean asymmetry seen in our data. The static asymmetry of HH 30 thus appears to have persisted for almost three decades. Furthermore, it may be possible to monitor changes in the asymmetry through ground-based polarimetric imaging.

In principle, a static disk asymmetry might be produced by spatially variable foreground extinction, either in the interstellar medium or in an envelope. Extended reflection nebulosity that may imply a circumstellar envelope is shown in Figure 1 of Burrows et al. (1996). The mean foreground extinction might be as large as 1.8 mag at *I*, and a small variation in this could produce a static asymmetry of the correct magnitude. However, spatially variable foreground extinction should produce a dramatically chromatic asymmetry: an asymmetry of +0.4 mag in *I* would be observed as an asymmetry of roughly +0.8 mag in *V*.

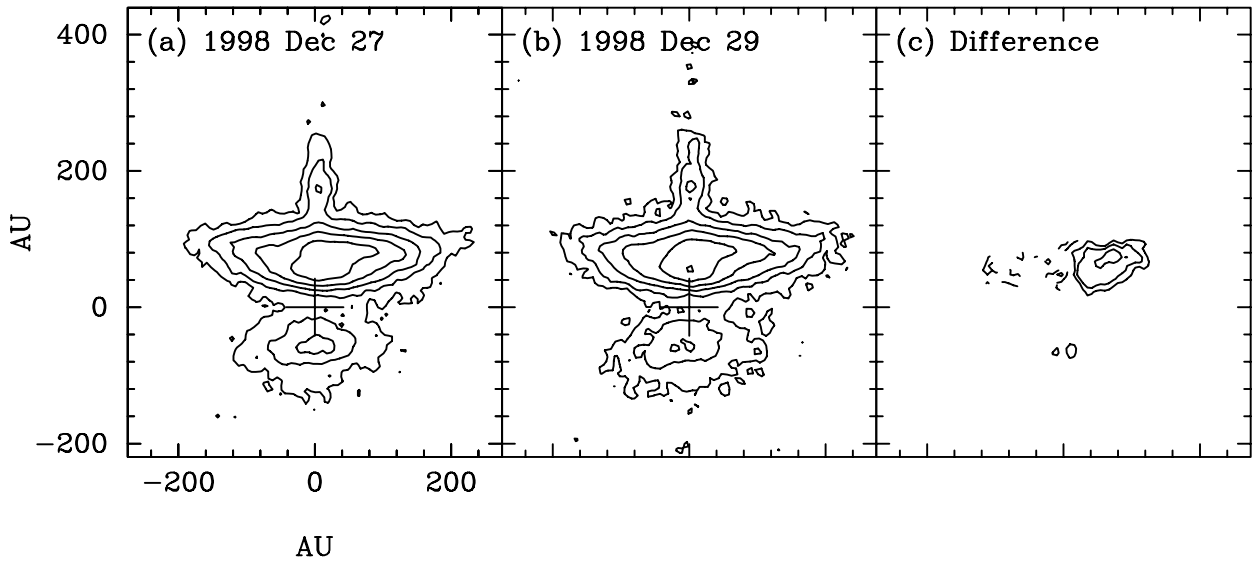

FIG. 14.—F555W images from (*a*) 1998 December 27 and (*b*) 1998 December 29, along with (*c*) the difference after the 1998 December 29 image was scaled to give the same m_u as the 1998 December 27 image. The images have been smoothed with a 2×2 boxcar filter to suppress noise. Positive and negative contours are spaced every 0.75 mag from 21.0 mag arcsec^{-2}. Negative contours are dashed.

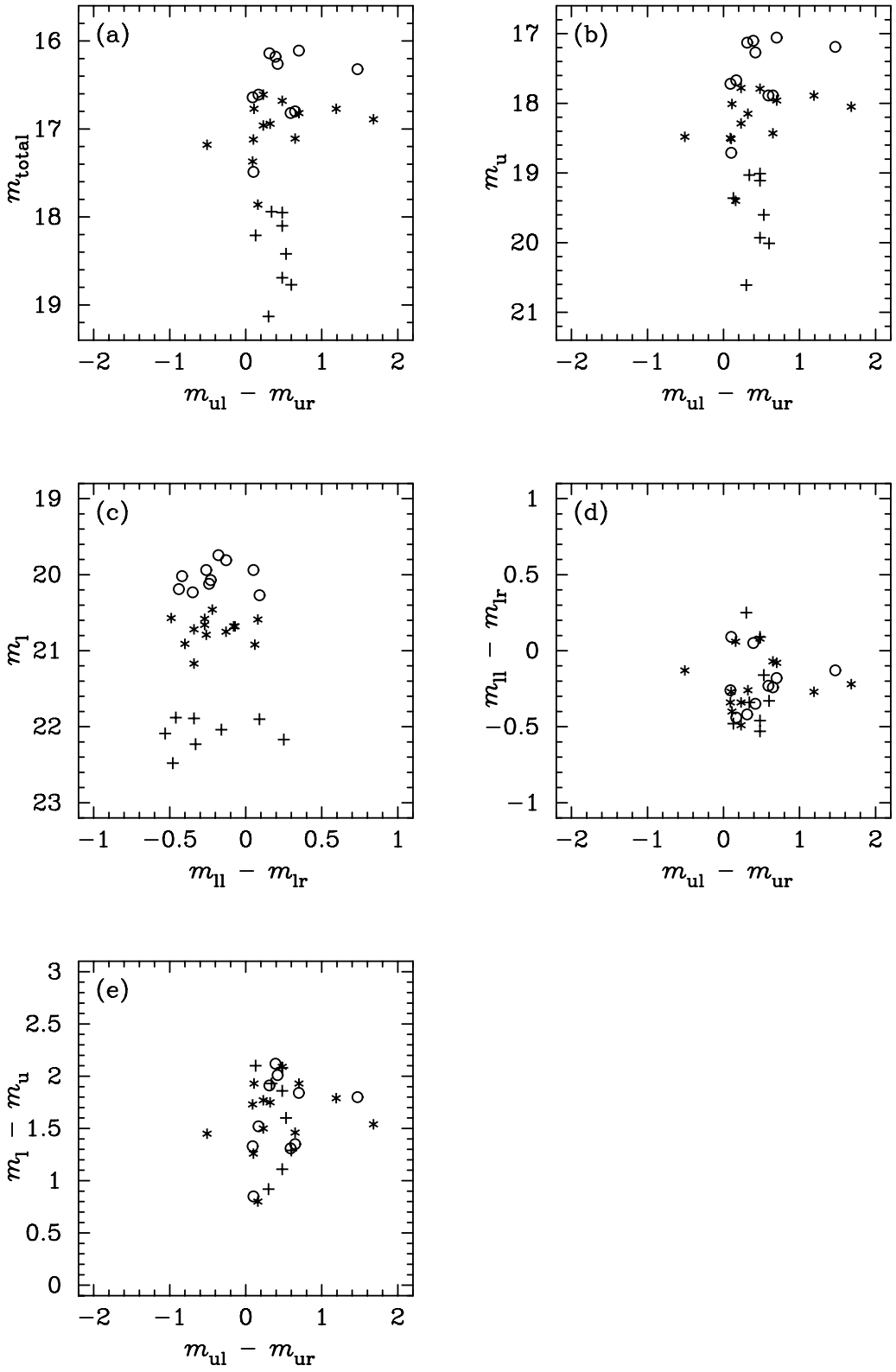

FIG. 15.—Plots showing the relations between the total magnitude $m_{\rm total}$, the magnitude of the upper nebulae m_u, the magnitude of the lower nebula m_l, the magnitude difference between the left and right sides of the upper nebula $m_{ul} - m_{ur}$, and the magnitude difference between the left and right sides of the lower nebula $m_{ll} - m_{lr}$. The symbols denote the filter: F555W or F547M (*plus signs*), F606W, F675W, or F625W (*asterisks*), and F814W (*circles*).

We see no evidence for such large differences in the asymmetry with wavelength (see § 4.4.1). This chromaticity could be avoided if the foreground extinction consisted of optically thick clumps, but there is no evidence elsewhere in the ISM for such extinction.

A static disk asymmetry might be produced directly by additional illumination by a binary companion with a separation of a few tens of AU or more and whose orbital plane is misaligned with that of the disk. In order to reproduce the sense of the asymmetry in the upper nebula, the companion would currently have

to be above the right side of the upper nebula. The separation of a few tens of AU would be required both to get a significant contrast between the left and right sides of the upper nebula at radii of 50–100 AU, and to maintain the vertical profile asymmetry over 10 yr. Unfortunately, while additional illumination can explain the long-term asymmetry in the upper nebula, it is difficult to see how it could directly produce a static asymmetry with the opposite sense in the lower nebula. For this reason, we do not favor direct illumination by a binary companion as the explanation for the static symmetry.

Another mechanism that might explain a static asymmetry is a warped disk. A warp could produce an asymmetry by one of two mechanisms. A warp in the inner part of the disk could shadow certain segments of the outer disk; a warp in the outer part of the disk could cause certain sectors of the disk to effectively flare more steeply, and thus intercept more starlight. The vertical profiles of the upper nebula support this second possibility, being consistent with the disk being more strongly flared on its upper right side. In either case, to maintain the vertical profile asymmetry over 10 yr, the precession period of a warp should be longer than about 40 yr. A warp with $m = 1$ would produce a point-symmetric static asymmetry when viewed from its nodes, but when viewed from other azimuths could produce an asymmetry that is stronger in the upper nebula than in the lower nebula. Such a disk warp might be produced by the gravity of an unseen stellar companion or massive protoplanet. Alternatively, it might trace variations in angular momentum over the history of infall onto the disk.

In the edge-on disk around HK Tau B the brightest parts of the upper and lower nebulae are displaced laterally by similar amounts at different epochs (Stapelfeldt et al. 1998; Koresko 1998), which suggests that it too has a static disk asymmetry similar to that in HH 30.

5.3. *Variable Lateral Asymmetry in the Upper Nebula*

In addition to identifying a static asymmetry, our observations have greatly improved the characterization of the short-term variable lateral asymmetry of HH 30. Its key characteristics are that it must be able to make one side of the upper nebula at least twice as bright as the other, in order to produce deviations in the asymmetry in the upper asymmetry of about 1 mag from the mean. It must do this without changing the color of the illumination. It is not dominated by lines. It also must occur on a short timescale, as we have seen it appear on one side, then the other, and then return in only 1 yr, and it must be capable of changing by 0.2 mag in only 2 days. Finally, the mechanism responsible for the variable asymmetry in the upper nebula *must not produce a similarly strong variable asymmetry in the lower nebula*.

Cotera et al. (2007) have identified strongly variable lateral asymmetries in NICMOS observations of the Haro 6-5B, DG Tau B, and IRAS 04302+2247 edge-on disks. The mechanisms we now discuss for the case of HH 30 are likely to be relevant to these other systems as well.

5.3.1. *Ejections*

The additional epochs of HH 30 images eliminate any lingering suspicion that the strong asymmetry seen in 1998 February (Stapelfeldt et al. 1999) could arise from some kind of ejection process. An outflow swift enough to create a strong asymmetry between 1995 and 1998 should have carried emission well outside the previously established boundaries of the nebula at subsequent epochs. However, the new images presented here, taken up to 7 yr later, show no changes in the extent of the nebulosity; the asymmetry remains confined within the preexisting nebula.

5.3.2. *Variable Foreground Asymmetry*

One might imagine that "filaments" of foreground extinction traveling across the line of sight might produce a variable asymmetry. However, we can reject this on the same basis that we rejected foreground extinction as a possible cause of the static asymmetry: it would produce a strong wavelength dependence on the strength of the asymmetry, and this is not seen. Furthermore, since the variable asymmetry is only seen strongly in the upper nebula, the filaments would have to pass only over the upper nebula.

5.3.3. *Binary Illumination Effects*

There is currently no evidence to suggest that HH 30 is anything other than a single star. However, if the system was an unrecognized binary, there are several ways in which the presence of a second star could act to produce a variable asymmetry in the disk nebulosity.

First, if an unseen companion star was embedded within the disk, then asymmetric illumination by two nonvariable stellar sources without disks could produce a periodic asymmetry. In order for stellar orbital motion to produce variable disk illumination on the observed timescales of days to years, the two stars would have to be located within a few AU of each other. While this could produce strong variable asymmetries in the inner disk, they would not do so in the outer disk seen by *HST*. Close stellar companions could only produce noticeable variable illumination in the outer disk if the stars were in contact or almost in contact, so that one star significantly shadows the other. However, such a configuration would lead to an equally strong variable asymmetry in the lower nebula, and this is not seen.

A second possibility is that the observed disk orbits a central binary, and the secondary star possesses its own circumstellar disk. The circumsecondary disk could then occult illumination from the primary. However, tidal truncation suggests that any such disk would have an outer radius of at most 1/3 of the separation of the two stars. The resulting shadow would then extend over at most 2 arctan $(1/3) \approx 40^\circ$ of the outer disk, and thus produce modulations between the two sides of the nebula that we estimate would be only at the 20% level. This is insufficient to produce a variable asymmetry of the magnitude we have observed. Furthermore, again, such a configuration should produce a variable asymmetry in the lower nebula.

A third binary scenario that could produce a strong asymmetry is that of a wide binary in which one or both stars were strongly variable. Strong variability is commonly observed in T Tauri stars and is attributed to variable accretion. However, the separation of the stars would have to be of order 100 AU to illuminate the left and right sides of the disk differently. If the orbit of the hypothetical binary were coplanar with the observed disk, this model would produce enhanced illumination on the same sides of the upper and lower nebulae simultaneously, which is not seen. On the other hand, if the binary orbit was not coplanar with the disk, one star would preferentially illuminate the upper right part of the circumbinary disk while the other would then preferentially illuminate the lower left part of the circumbinary disk. It seems difficult to be able to preferentially illuminate both the upper left and upper right parts of the circumbinary disk, although this is what is required to explain the variable asymmetry. Also, this model is inconsistent with the predominant accretion of the central star, as evidenced by a single jet source located at the center of the disk, and with the lack of correlation between the magnitude of the lateral asymmetry and the brightness of the upper nebula (§ 4.4.5 and Fig. 10).

5.3.4. *Flares*

Strong flares at random longitudes on the surface of the single central star could produce variable asymmetries in the disk. The sense of the resulting variable asymmetry would be expected to vary stochastically with equal probability of both senses. This is not observed.

However, the asymmetry is observed to have roughly the same color as the nebula as a whole. Thus, if flares are responsible for the variable asymmetry, they would also have to be responsible for the overall illumination of the nebula (i.e., they must dominate normal photospheric light). We are unaware of any other stars with this property.

5.3.5. *Stellar Accretion Hot Spots*

Wood & Whitney (1998) suggested that variable asymmetries in the HH 30 disk might originate through illumination of the disk by stellar accretion hot spots. These hot spots would be located at the star's north and south magnetic poles and mark the location where magnetically mediated accretion from the disk impacts the stellar surface. A stellar dipole field is assumed, with its axis inclined to the stellar rotation axis. As the star rotates, hot-spot illumination would then sweep across the outer disk. Our new data allow us to refine their suggestion.

The asymmetric hot-spot model makes a clear prediction for the periodicity in the nebula illumination: it should be equal to the stellar rotation period. YSO rotation periods are usually inferred from light curves under the assumption that fixed patterns of bright or dark surface spots rotate with the body of the star. For many YSOs no photometric period can be discerned, possibly because of the absence of spots, large stochastic variations, or the temporal sampling limitations of a typical observing run. However, among the T Tauri stars for which rotation periods have been determined, the periods are normally 12 days or less (Edwards et al. 1993; Bouvier et al. 1993), although there is a tail that stretches to longer periods (Rebull 2000). Our new data on the HH 30 variable asymmetry is consistent with a wide range of periods shorter than 300 days, and thus is consistent with the hot-spot model.

Wood et al. (2000b) obtained spatially unresolved photometry of HH 30 during late 1999 and early 2000 and published evidence for periods of 11.6 and 19.8 days. The 11.6 day period is spurious and results from an incorrect calculation of the periodogram (Watson & Durán-Rojas 2007, in preparation), but the 19.8 day period appears to be real. However, the 19.8 day period is intermittent and was not present in data obtained in early 1999 (Watson & Durán-Rojas 2007, in preparation) or late 2000 (Wood et al. 2000a). Our period analysis for the variable asymmetry has a gap in allowed periods between 18.7 and 20.1 days, which would seem to exclude a period of 19.8 days. However, this conclusion would be incorrect if the period is intermittent or if the asymmetry suffers phase shifts. Given the lack of correlation between the total light and the strength of the asymmetry (Fig. 15), it is not clear that a 19.8 day photometric period should be seen in the behavior of the variable lateral asymmetry.

The asymmetric hot-spot model also makes a clear prediction for the color of the asymmetry: it should be the same as the color of the hot spots. We observe very little color in the asymmetry in $V - I$. However, White & Hillenbrand (2004) also observed very little color difference in $R - I$ between the photosphere and the veiling components. (That is, the "hot spots" in HH 30 appear to be better described as "bright spots.") There appears to be no inconsistency here between the hot-spot model and the $V - I$ color of the asymmetry. There is also no inconsistency between the hot-spot model and the lack of line emission in the asymmetry.

Stapelfeldt et al. (1999) pointed out that point-symmetric hot spots should produce a large but opposite asymmetry in the lower nebula; this was not seen in the 1998 March image, which showed a very strong asymmetry in the upper nebula. Our additional data and modeling serve to strengthen the conclusion that any hot-spot model for the variability in HH 30 cannot be point symmetric. However, hot spots that are preferentially present on the upper surface of the star, such as might be produced by an offset and tilted dipole or other complex stellar magnetic field geometries, could still explain the temporal behavior of the lateral asymmetries in both nebulae.

One can argue that hot spots should produce a correlation between the amplitude of the lateral asymmetry and the brightness of the upper nebula (or the contrast between the upper and lower nebulae). However, maximum asymmetry should occur when the hot spot is roughly in the plane of the sky, at which point the upper nebula will have a brightness that is intermediate between its maximum (when the hot spot faces toward the observer) and minimum (when the hot spot faces away from the observer). Figure 15*e* seems to be consistent with this, with the largest variability in the lateral asymmetry coinciding with intermediate vertical contrasts. Figure 15*b* is less clear, perhaps because of additional global variability.

5.3.6. *Shadowing by the Inner Disk*

Density inhomogeneities in the inner disk could produce variable illumination patterns corresponding to the outer disk asymmetry seen with *HST*. These inhomogeneities could take the form of a spiral density wave or warp and might be associated with a companion star, brown dwarf, planet, or the magnetic field of the central star. The period of the asymmetry would correspond to the pattern period (or, in the case of asymmetries with $m > 1$, at a fraction $1/m$ of the pattern period) of the disturbance in the disk. The disk is relatively low mass and is unlikely to be self-gravitating, so this pattern period probably corresponds to the rotational or orbital period of whatever might be forcing the asymmetry. The range of allowed periods of up to about 300 days correspond to disturbances out to about to 1 AU.

On the other hand, a pure $m = 1$ point-symmetric distortion would produce a point-symmetric variability in the lower nebula, and this is not seen. Any shadowing mechanism has to produce variability in the upper nebula without producing strong variability in the lower nebula.

An inner disk inhomogeneity could only generate the observed lateral asymmetry if it provided a sufficiently large increase in the optical depth along the lines of sight to the outer disk at 100 AU. These lines of sight are inclined at 10°–20° to the equatorial plane. Since the disk scale height H decreases faster than R (H/r increases as $r^{1/8}$ to $r^{1/2}$) as one moves inward, it becomes progressively more difficult for the innermost parts of the disk to shadow the outer parts. A discontinuity in the scale height is expected at the disk inner edge, which corresponds to the radius of the dust destruction temperature. The inner edge of the disk will be frontally illuminated, and thus puffed-up relative to the rest of the flared disk, which is illuminated obliquely. Inhomogeneities at the inner rim have been suggested as an explanation for the photometric variability in UX Ori stars (Dullemond et al. 2003). A hydrostatically supported disk will have a Gaussian scale height $H(r) = [kT(r)r^3/GMm]^{1/2}$. For a stellar luminosity of 1 $L_\odot$ and $T = 1500$ K, the disk inner edge would be at $r = 0.04$ AU. For a 0.45 $M_\odot$ star

(Pety et al. 2006), the scale height would be 0.0014 AU, H/r would be 0.035, and the resulting shadow angle would be only 2°. Even if the $\tau = 1$ surface extended to many scale heights above the disk plane, it is unlikely that the inner rim would have sufficient vertical extent for any inhomogeneities there to produce visible effects on the outer disk.

Bouvier et al. (1999) have suggested that the photometric variations in AA Tau might be explained by occultations of the star by a warp in the inner disk caused by an inclined dipole magnetic field. Terquem & Papaloizou (2000) followed this up theoretically and showed that moderately inclined dipoles can produce warps of up to 10% of the disk inner radius. O'Sullivan et al. (2005) were able to model the photopolarimetry of AA Tau with a warped inner disk that casts a shadow over about 90° of azimuth. The period of the variable illumination would then equal the rotational period of the star. This model might well produce the observed asymmetry seen in HH 30, provided the $m = 1$ point symmetry can be broken, perhaps by offsetting the dipole from the star or by the influence of a binary companion. An inclined stellar dipole field could therefore produce periodic variable illumination on the outer disk through two distinct mechanisms: shadowing by the warped inner disk, or beaming from inclined stellar accretion hot spots. It is not clear how to distinguish between these two variable illumination mechanisms, as they should share the same stellar rotation period.

5.4. *Static Vertical Asymmetries*

There is a trivial asymmetry between the upper and lower nebulae: the system is inclined to the line of sight, with the upper nebula inclined slightly toward us and the lower nebula inclined slightly away from us. However, there are three other static asymmetries between the upper and lower nebulae. First, the upper nebula shows lateral variability, whereas the lower nebula does not. Second, the variability of the brightness of the lower nebula is only 0.7 mag whereas the variability of the upper nebula is 1.7 mag. Third, the outflow emanating from the upper nebula has a more collimated jet with a lower excitation (as traced by the [S II]/Hα ratio; Ray et al. 1996) and is stronger in molecular lines (Pety et al. 2006). A common explanation for these three differences is still to be found.

5.5. *Variable Vertical Asymmetry*

The contrast between the upper and lower nebulae of HH 30 is observed to vary by 1.3 mag and appears to be almost independent of color. It is interesting that the variable vertical asymmetry and the variable lateral asymmetry share a lack of color and have similar amplitudes. This suggests that both may be caused by a single mechanism. The lack of a clean correlation between the amplitude of the lateral asymmetry and the vertical contrast does not eliminate this possibility, as we discussed above in § 5.3.4 and § 5.3.5.

5.6. *Variability Implications for Disk Model Fitting*

HH 30 has been the subject of extensive modeling efforts by Burrows et al. (1996), Wood et al. (1998), Cotera et al. (2001), and Watson & Stapelfeldt (2004). In each case, the authors fitted models to images of HH 30 to constrain the opacity structure of the disk or the optical properties of the dust. Watson & Stapelfeldt explicitly symmetrized the disk image data about the jet axis prior to model fitting, whereas the other studies did not. All four studies assumed the disk was symmetric about a rotational axis and through the disk midplane. Their model illuminating sources had spherical symmetry and were located at the center of the disk.

The upper-lower and left-right variability will have two direct effects on parameters derived from fitting models. The upper-lower variability will directly affect the inclination derived for the disk. The left-right asymmetry will directly affect the value of the scattering asymmetry parameter g. There may well be secondary effects; for example, uncertainties in the inclination lead to uncertainties in the extinction to the star.

On the other hand, the vertical profile of the dark lane between the two nebulae does not seem to be significantly affected by the variability. This suggests that the constraints obtained by Cotera et al. (2001) and Watson & Stapelfeldt (2004) on the opacity law are robust, as these stem largely from the wavelength-dependent thickness of the dark lane.

5.7. *Implications for Polarimetry*

Monin et al. (1998, 2006) and Jensen et al. (2004) have used polarimetry to infer the relative orientations of the disks in young binary systems. However, the static lateral asymmetry and the variable lateral asymmetry in HH 30 could violate the fundamental assumption of this method: that the polarization vector is either perpendicular or parallel to the projected axis of the disk. Of course, this additional "noise" will not lead to a false positive result, but it may explain why a few stars have polarization vectors that are close but not perfectly aligned with each other.

6. CONCLUSIONS AND FUTURE WORK

Our analysis of *HST* observations from 18 epochs left us with a greater understanding of the photometric and morphological behavior of HH 30. We have summarized these results in § 4.5. Picking through these observational results, we identify vertical and lateral static asymmetries and vertical and lateral variabilities. These can be most simply explained by three components. First, there seems to be a static lateral asymmetry in the disk. Second, as in other accreting T Tauri stars, there is likely to be a global variability in the stellar illumination that affects all parts of the disk roughly equally. This could explain the 0.7 mag of variability in the lower nebula. Finally, there could be something close to the star that is able to produce a enhanced variability and a variable lateral asymmetry in the upper nebula, without producing these effects in the lower nebula. This would explain the 1.3 mag of variability in the contrast between the upper and lower nebulae and the roughly similar amplitude of the variable lateral asymmetry in the upper nebula. This mechanism might be an offset inclined magnetic dipole and its influence on accretion and the inner disk. This might also produce the difference in the jet between the upper and lower nebula. However, we note that an inclined dipole is likely to produce both an inclined warp and inclined hot spots, both of which could produce a variable asymmetry with the same period. Disentangling these two mechanisms might be difficult.

Further progress could be enabled through three types of observations. First, the temporal sampling of the data used by this study was sufficient to study variability on timescales of months and years, but was inadequate to identify any periodic effects on timescales of days or weeks. It is important to explore variability on these timescales and determine whether there is a modulation that could correspond to the stellar rotation period. Durán-Rojas and Watson have recently monitored the integrated polarization of HH 30 in I and might be able to resolve this point. Second, hot spots can be expected to produce their strongest photometric contrast to the stellar photosphere at short wavelengths such as B band. If the asymmetry were observed to be stronger in B than in I, for example, this would strongly favor illumination by hot

spots over shadowing by warps. Third, we need to explore other systems to determine whether the phenomena we have observed are unique to HH 30 or are more common. Cotera et al. (2007) have identified three other systems with variable lateral asymmetries; these need to be studied in detail.

The work is supported by NASA under *Hubble Space Telescope* GO grants 6754 and 9236 to the Jet Propulsion Laboratory and by CONACyT under project 27570E to the Universidad Nacional Autónoma de México. We thank Doug Van Orsow of the Space Telescope Science Institute, program coordinator for GO 6754, for his quick action after a guide star acquisition failure made it possible to get repeat observations scheduled immediately, thereby preserving the key 2 day interval in our observations. We thank John Krist and Chris Burrows for their help in the initial stages of this study, Wolfgang Brandner for his reduction of the 1997 HH 30 NICMOS image from the *HST* archive, and Angela Cotera for providing the 2005 ACS image prior to publication. We thank an anonymous referee for several thoughtful suggestions. Finally, we thank Paola D'Alessio, Will Henney, Bill Herbst, Scott Kenyon, Susana Lizano, Luisa Rebull, and Linda Sparke for discussions on certain points.

REFERENCES

Bouvier, J., Cabrit, S., Fernández, M., Martín, E. L., & Matthews, J. M. 1993, A&A, 272, 176
Bouvier, J., et al. 1999, A&A, 349, 619
Brandner, W., et al. 2000, A&A, 364, L13
Burrows, C. J. 1995, WFPC2 Instrument Handbook (3rd ed.; Baltimore: STScI)
Burrows, C. J., et al. 1996, ApJ, 473, 437
Cohen, M., & Schmidt, G. D. 1981, AJ, 86, 1228
Cotera, A. S., Schneider, G., Hines, D. C., Whitney, B. A., Stapelfeldt, K. R., & Padgett, D. L. 2007, AJ, submitted
Cotera, A., et al. 2001, ApJ, 556, 958
Dickinson, M. 1999, NICMOS Data Handbook (4th ed.; Baltimore: STScI)
Dullemond, C. P., van den Ancker, M. E., Acke, B., & van Boekel, R. 2003, ApJ, 594, L47
Edwards, S., et al. 1993, AJ, 106, 372
Herbst, W., Herbst, D. K., Grossman, E. J., & Weinstein, D. 1994, AJ, 108, 1906
Holtzman, J. A., Burrows, C. J., Casertano, S., Hester, J. J., Trauger, J. T., Watson, A. M., & Worthey, G. 1995a, PASP, 107, 1065
Holtzman, J. A., et al. 1995b, PASP, 107, 156
Jensen, E. L. N., Mathieu, R. D., Donar, A. X., & Dullihan, A. 2004, ApJ, 600, 789
Koresko, C. D. 1998, ApJ, 507, L145
Monin, J.-L., Ménard, F., & Duchêne, G. 1998, A&A, 339, 113
Monin, J.-L., Ménard, F., & Peretto, N. 2006, A&A, 446, 201
O'Sullivan, M., Truss, M., Walker, C., Wood, K., Matthews, O., Whitney, B., & Bjorkman, J. E. 2005, MNRAS, 358, 632
Pety, J., Gueth, F., Guilloteau, S., & Dutry, A. 2006, A&A, submitted
Ray, T. P., Mundt, R., Dyson, J. E., Falle, S. A. E. G., & Raga, A. C. 1996, ApJ, 468, L103
Rebull, L. 2000, Ph.D. thesis, Univ. Chicago
Stapelfeldt, K. R., Krist, J. E., Ménard, F., Bouvier, J., Padgett, D. L., & Burrows, C. J. 1998, ApJ, 502, L65
Stapelfeldt, K. R., & Moneti, A. 1999, in The Universe as Seen by *ISO*, ed. P. Cox & M. Kessler (ESA SP-427; Noordwijk: ESA), 521
Stapelfeldt, K. R., & Padgett, D. L. 2001, in ASP Conf. Ser. 235, Science with the Atacama Large Millimeter Array, ed. A. Wooten (San Francisco: ASP), 163
Stapelfeldt, K. R., et al. 1999, ApJ, 516, L95
Strom, K. M., Strom, S. E., Edwards, S., Cabrit, S., & Skrutskie, M. F. 1989, AJ, 97, 1451
Terquem, C., & Papaloizou, J. C. B. 2000, A&A, 360, 1031
Thé, P. S., Steenman, H. C., & Alcaino, G. 1984, A&A, 132, 385
Watson, A. M., & Stapelfeldt, K. R. 2004, ApJ, 602, 860
White, R. J., & Hillenbrand, L. A. 2004, ApJ, 616, 998
Whitney, B. A. 1995, in Rev. Mex. AA Ser. Conf., 1, 201
Whitney, B. A., & Hartmann, L. 1992, ApJ, 395, 529
Wood, K., Kenyon, S. J., Whitney, B., & Turnbull, M. 1998, ApJ, 497, 404
Wood, K., Stanek, K. Z., Wolk, S. J., Whitney, B. A., & Stassun, K. G. 2000a, BAAS, 32, 1414
Wood, K., & Whitney, B. 1998, ApJ, 506, L43
Wood, K., Wolk, S. J., Stanek, K. Z., Leussis, G., Stassun, K., Wolff, M., & Whitney, B. 2000b, ApJ, 542, L21